Intense laser-field ionization of H_2 enhanced by two-electron dynamics

Kenji Harumiya, Hirohiko Kono, and Yuichi Fujimura
Department of Chemistry, Graduate School of Science, Tohoku University, Sendai 980-8578, Japan

Isao Kawata and André D. Bandrauk
Laboratoire de Chimie Théorique, Faculté des Sciences, Université de Sherbrooke, Sherbrooke, Québec, Canada J1K 2R1

(Received 10 June 2002; published 4 October 2002)

Intramolecular electronic dynamics and tunnel ionization of H_2 in an intense laser field ($I \approx 10^{14}$ W/cm^2 and $\lambda = 760$ nm) are examined with accurate evaluation of three-dimensional two-electron wave-packet dynamics by the dual transformation method. We estimated the ionization probabilities at different values of the internuclear distance R and found that tunnel ionization of H_2 is enhanced by field-induced two-electron dynamics. An ionic component characterized by the electronic structure H^+H^- or H^-H^+ is created near the descending well, where the dipole interaction energy with the laser electric field $\varepsilon(t)$ becomes lower. Ionization proceeds via the formation of a localized ionic component in the descending well, in contrast to the H_2^+ case, in which the electron is ejected most easily from the ascending well. As R increases, while the population of H^-H^+ (or H^+H^-) decreases, a pure ionic state H^-H^+ becomes easier to ionize in an intense field because of the smallar attractive force of the distant nucleus. As a result, ionization is enhanced at the critical distance $R_c = (4-6)a_0$ (a_0 is the Bohr radius). Although the rate of direct ionization from a covalent state is much smaller than that from an ionic state, the ionization at large R ($\geqslant 8a_0$) mainly proceeds from the remaining covalent component, which outmeasures the created ionic component. Thus, the field-induced intramolecular electron transfer between nuclei, which triggers strong electron-electron correlation, is governed by the molecular structure as well as the field intensity. The mechanism of the ionization enhanced by field-induced intramolecular electron transfer is consistent with the observation of charge-asymmetric dissociation channels of diatomic molecules such as $N^+ + N^{3+}$. We also investigated the intramolecular electronic dynamics by analyzing the populations of field-following adiabatic states defined as eigenfunctions of the instantaneous electronic Hamiltonian. An effective instantaneous Hamiltonian for H_2 was constructed of three main electronic states, X, $B\ ^1\Sigma_u^+$ and EF. We found that the difference in electronic and ionization dynamics between the small R and large R cases originates in the character of the level crossing of the lowest two adiabatic states.

DOI: 10.1103/PhysRevA.66.043403 PACS number(s): 33.80.Rv, 33.80.Wz, 42.50.Hz

I. INTRODUCTION

The development of high-power lasers has opened up the research field of nonperturbative phenomena in intense fields such as above-threshold ionization [1–3] and higher-order harmonic generation of emission [2–5]. In a high-intensity and electronically nonresonant long-wavelength regime (intensity $I > 10^{13}$ W/cm^2 and wavelength $\lambda > 700$ nm), a laser electric field significantly distorts the Coulombic potential that the electrons are placed in. The distorted potential forms a quasistatic barrier (or barriers) through which an electron or electrons can tunnel [3,6,7]. This type of ionization is called tunnel ionization. In the case of atoms, such nonperturbative phenomena can be understood in terms of quasistatic models [8–10]. The quasistatic tunneling condition is given by the inequality $\gamma < 1$, where γ is the Keldysh parameter [6].

Interest has recently been shown in the role of interelectronic correlation in intense fields. Momentum distributions of photoelectrons and recoil ions in nonsequential double ionization of He and Ar atoms have been reported [11,12]. The validity of correlation mechanisms such as ''rescattering'' [8], ''antenna'' [13], and ''shake-off'' proposed to explain nonsequential double ionization has been tested by different theoretical approaches. By incorporating the electron-electron repulsion term into the so-called intense-field many-body S-matrix theory, Becker and Faisal [14] reproduced the measured momentum distribution of doubly charged He^{2+} ions. The rescattering and antenna models are unified in the ''energy-sharing'' mechanism proposed, namely, that the photon energy absorbed by one electron is shared with the other electron via the interelectronic correlation. The mechanism of nonsequential double ionization has also been examined by numerically solving the time-dependent Schrödinger equation of He [15].

Compared to atoms, molecules in intense fields exhibit complex phenomena arising from their additional (vibrational and rotational) degrees of freedom, such as charge-symmetric and -asymmetric dissociation [16–18], alignment with an external field [19], creation of electronically excited fragments [20,21], and ionization rates that depend on the internuclear distance (enhanced ionization of molecules) [17,22–24]. In the case of molecules, a large part of the electron density can be transferred among nuclei within one-half optical cycle of an intense field [25–31]. It is expected that such intramolecular electronic motion will enhance the subsequent tunnel ionization. Field-induced ultrafast electron transfer also triggers nuclear motion [28–32]. The resultant structure deformations in turn change the electronic response to the field, e.g., intramolecular electron transfer followed by tunnel ionization. Enhanced ionization has been experimentally observed for various molecules such as CO_2 [33] and benzene molecules [34]. The internuclear distance at which ionization occurs, called the critical distance, is deduced by

assuming that the released kinetic energy of a pair of fragment ions comes from the potential energy of the Coulomb repulsion of the ion charges. The critical distance R_c deduced is a few times larger than the equilibrium internuclear distance R_e [35].

Theoretical explanations for enhanced ionization started with one-electron systems such as H_2^+ and H_3^+. Recent accurate numerical simulations of ionization showed that the ionization rate is maximum at a critical internuclear distance R_c and far exceeds the ionization rate of the neutral fragment H [36–39]. The instantaneous electrostatic potential for the electron in H_2^+ has two wells around the nuclei. The dipole interaction energy for an electron is $\varepsilon(t)R/2$ at the right nucleus and $-\varepsilon(t)R/2$ at the left nucleus, where $\varepsilon(t)$ is the laser electric field at time t and R is the internuclear distance. As $\varepsilon(t)$ increases from zero, the potential well formed around the right nucleus ascends and the well formed around the left nucleus descends. Therefore, the ascending and descending wells yield the field-following adiabatic states $|+\rangle$ and $|-\rangle$, respectively. In addition to the barrier between the two wells (inner barrier), a barrier with finite width for electron tunneling is formed outside the descending well when $|\varepsilon(t)| \neq 0$ (outer barrier). While the adiabatic energy E_- of $|-\rangle$ is usually below the barrier heights, E_+ can be higher than the barrier heights in the range $R_c=(6-9)a_0$ [29–31,36–39]. In this critical range of R, the upper adiabatic state $|+\rangle$ is easier to ionize than is $|-\rangle$ [30,36,39]. After one-electron ionization from H_2, the bond distance of the resultant H_2^+ stretches in the E_- laser-induced dissociative potential [29–31,40,41], and then ionization proceeds via the $|+\rangle$ state (from the ascending well) that is nonadiabatically created around R_c from $|-\rangle$ when the field $\varepsilon(t)$ changes its sign (i.e., electron transfer between the nuclei is suppressed). This type of ionization of H_2^+ is called charge resonance-enhanced ionization [36]. In the case of two-electron molecules, however, different mechanisms can be expected because the two electrons are forced to move in a correlative way by an intense laser field.

In molecules, interelectronic correlation in an intense field takes on a different aspect associated with the molecular structure; field-induced intramolecular electron transfer between nuclei triggers strong electron-electron correlation. For H_2, localized ionic bond states H^+H^- and H^-H^+ are expected to be created in an intense field [27,42,43]. The formation of localized ionic states should be related to the mechanism of ionization of H_2. Elucidation of this relationship is a key to answering the question as to how interelectronic correlation and molecular structure affect each other in intense fields. It is expected that the clarified mechanism of enhanced ionization for two-electron molecules would serve as a prototype of tunnel ionization of multielectron molecules. We also expect that the formation of localized ionic states is closely related to the mechanism of nonsequential double ionization of molecules [44–46].

In previous studies [42,43], we analyzed the ionization process for a one-dimensional (1D) H_2 molecule in an intense, low-frequency laser field (intensity $I \geqslant 10^{14}$ W/cm^2 and $\lambda = 1064$ nm) by numerically solving the time-dependent Schrödinger equation. In the calculations, the two electrons are allowed to move in a regularized (softened) Coulombic potential only along the molecular axis. According to the 1D model calculation, the laser field forces the two electrons to stay near a nucleus for one-half cycle, and the resultant transient ionic structures such as H^-H^+ and H^+H^- are the main doorway states to tunnel ionization. Maxima in the ionization rate with respect to R have been found for the 1D H_2 model. The 1D calculated surfaces and transition moments relevant to main electronic states qualitatively agree with accurate calculations for 3D H_2, except that the 1D potentials are all shifted down [42]. Although these features validate the use of the 1D model, 3D calculation is indispensable for quantifying the role of two-electron dynamics in enhanced ionization. It should be pointed out that ambiguous parameters are introduced to remove the Coulomb singularity in the 1D model. Generally speaking, the 3D and 1D models give different populations of H^-H^+ and different ionization rates. The localized ionic structure H^-H^+ geometrically has more different forms in the 3D model than in the 1D model.

To quantitatively understand the electronic dynamics of two-electron molecules in intense fields, it is necessary to solve the time-dependent Schrödinger equation for the electronic degrees of freedom of a molecule [47]. We have developed an efficient grid point method, the dual transformation method [48], for accurate propagation of the 3D electronic wave packet of a small molecular system such as H_2^+ [28] or H_2 [27]. To the best of our knowledge, our treatment of H_2 is the first accurate evaluation of two-electron correlation dynamics of a molecule. The electron correlation is ignored or only partially taken into account in the single active electron approximation [49] and the time-depenedent density functional method [50]. In this paper, we present the results of calculation of electronic wave-packet dynamics of a 3D H_2 model in a long-wavelength intense field and show that tunnel ionization of H_2 is enhanced by field-induced two-electron dynamics.

The rest of this paper is organized as follows. Derivation of a 3D H_2 Hamiltonian suitable for calculating the wave-packet dynamics in an intense, linearly polarized laser field is presented in Sec. II. In Sec. III, the results of numerical simulation of the electronic wave-packet dynamics of the 3D H_2 model are presented, and the dependence of the ionization probability on R is discussed. The intramolecular electronic dynamics leading to the formation of localized ionic states prior to ionization is analyzed by means of ''field-following'' adiabatic states $\{|n(t)\rangle\}$ [28–31] . Those states are defined as eigenfunctions of the ''instantaneous'' electronic Hamiltonian $H_0(t)$ including the interaction with $\varepsilon(t)$. Finally, in Sec. IV, a brief summary of the results of the present work is given together with concluding remarks.

II. DERIVATION OF A HAMILTONIAN OF H_2

We briefly describe the derivation of a H_2 Hamiltonian suitable for calculating the electronic wave-packet dynamics in an intense laser field [27]. The position of each electron is designated by cylindrical coordinates (ρ,z, and φ). The z axis is parallel to the molecular axis (the origin of the z axis

being located at the midpoint between the two nuclei). Here, we assume that the two nuclei are fixed in space at a given internuclear distance R and that the molecular axis is aligned by a linearly polarized laser electric field $\varepsilon(t)$ [19]. The z axis is thus parallel to the polarization direction (parallel polarization condition). We first define a one-electron Hamiltonian $\hat{H}_j$ for the jth electron:

$$\hat{H}_j = -\frac{1}{2}\left(\frac{\partial^2}{\partial\rho_j^2}+\frac{1}{\rho_j}\frac{\partial}{\partial\rho_j}+\frac{\partial^2}{\partial z_j^2}\right)+V(\rho_j,z_j)+z_j\varepsilon(t), \quad (1)$$

where the last term is the dipole interaction of the jth electron with the field $\varepsilon(t)$, and $V(\rho_j,z_j)$ represents the Coulomb attraction between the jth electron and the nuclei:

$$V(\rho,z) = -\frac{1}{\sqrt{\rho^2+(z-R/2)^2}}-\frac{1}{\sqrt{\rho^2+(z+R/2)^2}}. \quad (2)$$

Throughout this paper, atomic units are used in the equations. The length is given in units of the Bohr radius a_0 and the energy is given in units of the Hartree energy E_H.

If the kinetic energy originating from the z component of the angular momentum, $-(1/2)\rho_j^{-2}\partial^2/\partial\varphi_j^2$, is added to $\hat{H}_j$, we obtain the Hamiltonian of H_2^+ [28]. Thus, the total Hamiltonian of H_2 can be expressed as

$$\hat{H} = \sum_{j=1}^{2}\hat{H}_j+\left[-\left(\sum_{j=1}^{2}\frac{1}{2\rho_j^2}\frac{\partial^2}{\partial\varphi_j^2}\right)+V_{12}(\{\rho_j\},\{z_j\},\{\varphi_j\})\right], \quad (3)$$

where V_{12} is the electron-electron repulsion:

$$V_{12}(\{\rho_j\},\{z_j\},\{\varphi_j\}) = \frac{1}{\sqrt{\rho_1^2+\rho_2^2-2\rho_1\rho_2\cos(\varphi_1-\varphi_2)+(z_1-z_2)^2}}. \quad (4)$$

Introducing the relative angle ϕ between the two electrons,

$$\phi = \varphi_1-\varphi_2, \quad (5)$$

and the average χ,

$$\chi = (\varphi_1+\varphi_2)/2, \quad (6)$$

we can rewrite the two-electron part $[\cdots]$ in Eq. (3) as

$$\hat{H}_{12} = -\frac{1}{2}\left(\frac{1}{\rho_1^2}+\frac{1}{\rho_2^2}\right)\left(\frac{\partial^2}{\partial\phi^2}+\frac{\partial^2}{4\partial\chi^2}\right)-\frac{1}{2}\left(\frac{1}{\rho_1^2}-\frac{1}{\rho_2^2}\right)\frac{\partial}{\partial\chi}\frac{\partial}{\partial\phi}+V_{12}(\{\rho_j\},\{z_j\},\phi). \quad (7)$$

Since the z axis component of the total angular momentum is conserved for the parallel polarization condition, the wave function takes the product form of $e^{i\ell\chi}$ and a function $\Phi(\{\rho_j\},\{z_j\},\phi)$, where ℓ is the quantum number for the z component of the total angular momentum. The range of χ is between 0 and 2π: the allowed values are $\ell=0, \pm1, \pm2, \ldots$. Thus, the total Hamiltonian $\hat{H}(\ell)$ for $\Phi(\{\rho_j\},\{z_j\},\phi)$ is the sum of $\hat{H}_1+\hat{H}_2$ and the two-electron part $\hat{H}_{12}(\ell)$ obtained by replacing $\partial/\partial\chi$ in Eq. (7) with $i\ell$.

We have developed an efficient grid point method, the dual transformation method, for accurate propagation of an electronic wave packet [26–28]. In this method, both the wave function and the Hamiltonian are transformed to Ψ and $\hat{H}^T(\ell)$ consistently so that the numerical difficulties arising from the divergence of the Coulomb potentials are overcome. The time integration of the Schrödinger equation $i\Psi/\partial t = \hat{H}^T(\ell)\Psi$ is carried out using the alternating-direction implicit (ADI) formula [51]. The time step used is $\Delta t = 0.05\ \hbar/E_H$. The grid end points are chosen as $\rho_{max} = 5a_0$ and $z_{max} \approx -z_{min} \approx 12a_0$. At the grid boundaries, Ψ is set to zero. The numerical procedure has been described in detail in Refs. [27,28,48].

III. RESULTS AND DISCUSSION

In this section, we present the results of investigation of the two-electron wave-packet dynamics of H_2 in an intense linearly polarized field. The initial state at $t=0$ is the ground state $X\,^1\Sigma_g^+$ with $\ell=0$. The "exact" initial state can be obtained by operating a Hanning spectral filter $W(|\hat{H}(\ell=0)-E_0|)$ on an approximate initial state Φ^A [52]:

$$W(|\hat{H}(\ell=0)-E_0|) = \mathrm{Re}\int_0^\tau [1+\cos(\pi t/\tau)] \times \exp\{-it[\hat{H}(\ell=0)-E_0]\}dt, \quad (8)$$

where the field strength $\varepsilon(t)$ in $\hat{H}(\ell=0)$ is set to zero. The filter W is a monotonically decreasing function of the argument. The width of W is given by $1/\tau$. When E_0 is chosen to be near the exact energy of the initial state, the operation of W on Φ^A diminishes the components other than the "exact" initial state contained in Φ^A. Using the trapezoidal rule for the above integration, the operation of W on Φ^A is reduced to operations of the short-time propagator based on the ADI formula.

In this paper, we employ the following function Φ_X^A as a trial function for the state X:

$$\Phi_X^A(1,2) \propto a(1)b(2)+b(1)a(2), \quad (9)$$

where a and b denote the $1s$ atomic orbitals on the right proton and the left proton, respectively, and 1 and 2 represent the coordinates of the two electrons. The above approximate ground state meets the required conditions that the exact X state must possess: $\ell=0$ and a symmetric property of electron interchange. The spatial wave function must be symmetric with respect to interchange of the two electrons 1 and 2: $\Phi(\rho_1,\rho_2,z_1,z_2,\phi) = \Phi(\rho_2,\rho_1,z_2,z_1,-\phi)$ for the singlet state.

A. Electronic wave-packet dynamics at different internuclear distances

Although the molecular axis is assumed to be parallel to the polarization direction, the two-electron wave function

still has five degrees of freedom, z_1, z_2, ρ_1, ρ_2, and $\phi = \varphi_1 - \varphi_2$. Here, to represent the wave packet, we employ the reduced density $\bar{P}(z_1, z_2)$ obtained by integrating the square of the wave function $|\Phi(t)|^2$ over the degrees of freedom other than z_1 and z_2 parallel to the polarization direction [27]:

$$\bar{P}(z_1, z_2) = \int_0^\infty d\rho_1 \int_0^\infty d\rho_2 \int_0^{2\pi} d\phi \rho_1 \rho_2 |\Phi(\rho_1, \rho_2, z_1, z_2, \phi)|^2. \tag{10}$$

This representation is useful because, as will be discussed later, the electronic dynamics in H_2 is characterized by electron motion along the polarization direction z. The covalent bond configurations $(H \cdot H)$ around $z_1 = -z_2 = \pm R/2$ and the ionic bond configurations ($H^- H^+$ and $H^+ H^-$) around $z_1 = z_2 = \pm R/2$ can be distinguished by using Eq. (10). As an example, $\bar{P}(z_1, z_2)$ for the exact ground state $X\,{}^1\Sigma_g^+$ at $R = 4a_0$ is drawn in Fig. 1(a). The reduced density map clearly demonstrates that the covalent components around $z_1 = -z_2 = \pm R/2$ are dominant in the ground state at $R = 4a_0$. The localized ionic components $|H^+ H^-\rangle$ and $|H^- H^+\rangle$ contained in $\Phi(t=0)$ are both 19%, where the electronic states of $|H^+ H^-\rangle$ and $|H^- H^+\rangle$ are defined as H^- ions of which the centers are located at $z_1 = z_2 = \pm R/2$ (in the calculation of the H^- state, electron-electron repulsion is taken into account).

The field $\varepsilon(t)$ that the H_2 interacts with is assumed to be $f(t)\sin(\omega t)$, where ω is the frequency, and the pulse envelope $f(t)$ is linearly ramped with time t so that $f(t)$ attains its maximum f_0 after one cycle. The field parameters used are as follows: $f_0 = 0.12 E_H/ea_0$ ($I = 5.04 \times 10^{14}$ W/cm^2) and $\omega = 0.06 E_H/\hbar$ ($\lambda = 760$ nm). The instantaneous field strength is $\varepsilon(t) = 0.03 E_H/ea_0$ at $t = \pi/2\omega$ (which corresponds to $I = 3.15 \times 10^{13}$ W/cm^2); $\varepsilon(t) = -0.09 E_H/ea_0$ at $t = 3\pi/2\omega$ ($I = 2.84 \times 10^{14}$ W/cm^2).

To quantify the ionization probability, we use the overlap of the wave packet with the initial state (accurate calculation of the ionization probability of H_2 in an alternating field requires a huge memory and computational time). In the low-frequency regime, the population of the initial state at the moment when the field returns to zero [time t at which $\varepsilon(t) = 0$ is satisfied], $P_{init}(t)$, is expected to be correlated with the ionization probability $P_I(t)$ as a function of time. It is convenient to define $P_I(t)$ only at $\varepsilon(t) = 0$ as the bound state component, i.e., the population outside the Hilbert space constructed of the bound states of the zero-field electronic Hamiltonian. For the 1D model of H_2, in which the electrons are allowed to move only along the molecular axis, we have confirmed that at $\varepsilon(t) = 0$ the quantity $1 - P_{init}(t)$ is more or less equal to $P_I(t)$ and that the decay rate of the norm in the grid space enclosed with an absorbing boundary, regarded as the ionization rate, is equal to the decay rate of the initial state except in the region of $R \approx 4a_0$. In the following, we employ $1 - P_{init}(t)$ defined at $\varepsilon(t) = 0$ instead of $P_I(t)$. A further discussion of this treatment will be given in Sec. III C.

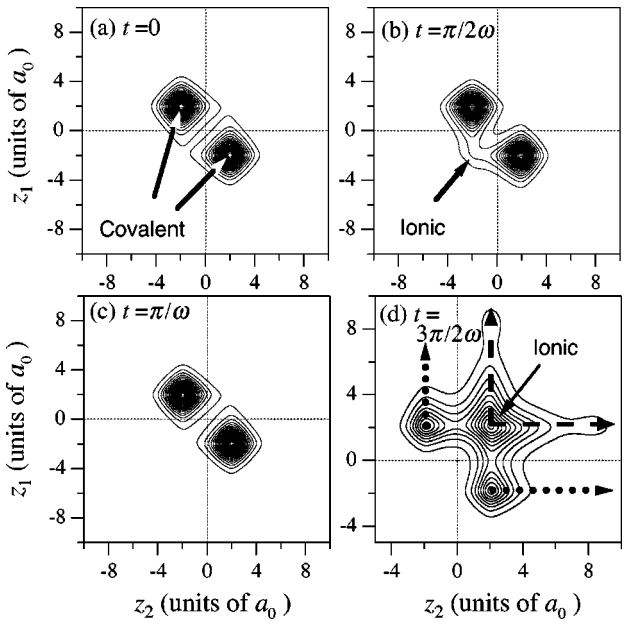

FIG. 1. Electronic wave-packet dynamics of H_2 in an intense field. The internuclear distance is fixed at $R = 4a_0$. The reduced density $\bar{P}(z_1, z_2)$ defined by Eq. (10) is drawn at quarter cycle intervals (the frequency of the applied field is $\omega = 0.06 E_H/\hbar$): (a) $t = 0$; (b) $t = \pi/2\omega = 26.2\hbar/E_H$; (c) $t = \pi/\omega$; (d) $t = 3\pi/2\omega$. The contour lines in the four panels are plotted at the same intervals. The field strength is $\varepsilon(t) = 0.03 E_H/ea_0$ at $t = \pi/2\omega$ and $\varepsilon(t) = -0.09 E_H/ea_0$ at $t = 3\pi/2\omega$. The initial state shown in (a) is the covalent character-dominated ground state X around $z_1 = -z_2 = \pm R/2$. The ionic component $H^- H^+$ around $z_1 = z_2 = -R/2$ (at the left nucleus) increases as the field approaches the first local maximum at $t = \pi/2\omega$, as shown in (b). The wave packet at $\varepsilon(t = \pi/\omega) = 0$ in (c) is nearly identical to the initial one in (a). In (d) the density around the ionic configuration ($z_1 = z_2 = R/2$) becomes very high because of the stronger field strength at $t = 3\pi/2\omega$. As indicated by the broken line in (d), an electron is ejected from the localized ionic structure. The direct ionization current from the covalent structure denoted by the dotted lines in (d) is relatively small.

We have calculated the wave-packet dynamics at different values of R. The initial state is the ground electronic state X. The relative ionization rates estimated from $1 - P_{init}$ for different values of R are shown in Table I. The field strength is zero both at $t = \pi/\omega$ and at $2\pi/\omega$. We consider the relative ionization rates in the first row in Table I to be those for the field $f(t) \approx f(t = \pi/2\omega)$ (the average field envelope between $t = 0$ and π/ω); the relative ionization rates in the second row are considered to be those for the field $f(t) \approx f(t = 3\pi/2\omega)$.

1. $R = 4a_0$

Snapshots of $\bar{P}(z_1, z_2)$ for $R = 4a_0$ are shown in Fig. 1: (a) $t = 0$; (b) $t = \pi/2\omega = 26.2\hbar/E_H = 0.634$ fs ($\hbar/E_H = 0.0242$ fs); (c) $t = \pi/\omega$; (d) $3\pi/2\omega$. In a low-frequency intense field, an ionic component is created around the descending potential well, where the electrostatic potential for

TABLE I. Estimated relative ionization rates for the applied field at various internuclear distances.

	R			
	$1.6a_0$	$4a_0$	$6a_0$	$8a_0$
From $1-P_{init}$ at $t=\pi/\omega$	1/110	18/110	15/110	4/110
From $1-P_{init}$ at $t=2\pi/\omega$	1	13	5	3

each electron, $z_1\varepsilon(t)$ or $z_2\varepsilon(t)$, is negative. For instance, the left well where z_1 and $z_2 \approx -R/2$ is the descending well when $\varepsilon(t)>0$. As the field approaches $t=\pi/2\omega$, the ionic component created around the left nucleus ($z_1=z_2=-R/2$) increases to $|\langle\Phi|H^-H^+\rangle|^2=0.31$. Note that $\varepsilon(t=\pi/2\omega)>0$. The corresponding reduced density map is shown in Fig. 1(b). The laser field forces the two electrons to stay near a nucleus for almost one half cycle. When the field returns to zero at $t=\pi/\omega$, the packet shown in Fig. 1(c) is almost identical to the initial one shown in Fig. 1(a), indicating that the response to the field is basically adiabatic.

Until then, no ionization current is observed on the scale of the contour line intervals. A quarter cycle later, at $t=3\pi/2\omega$, as shown in Fig. 1(d), the density around $z_1=z_2=R/2$ becomes as large as $|\langle\Phi|H^+H^-\rangle|^2=0.54$ because of the stronger field $\varepsilon(t=3\pi/2\omega)=-0.09E_H/ea_0$. From 3D analysis of the spatial configuration of the two electrons, we have also confirmed that the ionic component in the descending well (around $z_1=z_2=R/2$) is the H^- ion at the nucleus where the dipole interaction energy is lower. In the case of $R=4a_0$, the population of a localized ionic component is maximized around the time when the absolute value of the field strength takes a local maximum; then the population of the counterlocalized ionic component is minimized. The increase in a localized ionic component is caused by the loss of the counterlocalized ionic component through an intermediate covalent configuration. The field-following increase or decrease in the localized ionic components means that the response of the bound state component to the field is still adiabatic.

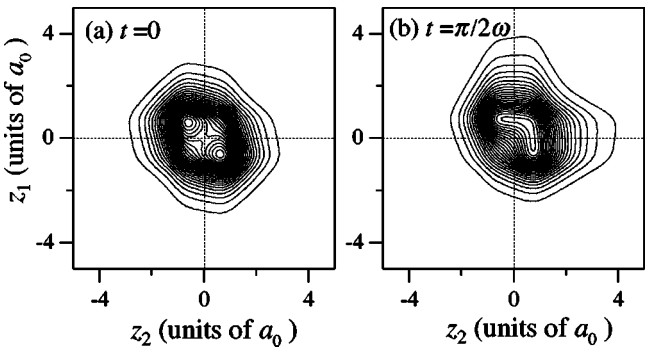

FIG. 2. Snapshots of the reduced density of H_2 at $R=1.6a_0$: (a) $t=0$, (b) $t=3\pi/2\omega$. The applied pulse is the same as that used in Fig. 1. Despite the intense field strength at $t=3\pi/2\omega$, the ionization current is very small.

As indicated by the broken line in Fig. 1(d), an electron is ejected from the localized ionic structure $|H^+H^-\rangle$. If the two nuclei are distant from each other, the ionization potential of the localized ionic structure is considered to be as low as the ionization potential of H^-, $I_p(H^-)=0.027E_H=0.75$ eV. The localized ionic structure is hence unstable and is regarded as a doorway state to ionization. The direct ionization route from a covalent structure is denoted by a dotted line in Fig. 1(d), but the current along the dotted line is relatively small. At $R=4a_0$, the rate of ionization from a pure ionic state is at least five times greater than that from a pure covalent state (deduced from the ionizing flux).

2. $R=1.6a_0$

The reduced densities at $t=0$ and $3\pi/2\omega$ for $R=1.6a_0$ ($\approx R_e=1.4a_0$) are shown in Figs. 2(a) and 2(b). Despite the intense field strength at $t=3\pi/2\omega$, the ionization current is very small. From Table I, we estimate that the change in R from $1.6a_0$ to $4a_0$ would enhance the ionization rate by a factor of 10–20. This is consistent with the ionization rates of the lowest adiabatic state in static fields calculated by Saenz [53]. He has reported that the ionization rate in a static field of $\varepsilon=0.08E_H/ea_0$ increases from $R=1.6a_0$ to $4a_0$ by a factor of 40.

For $R=1.6a_0$, $|\langle\Phi|H^+H^-\rangle|^2$ is as large as 0.74 at $t=3\pi/2\omega$, while $|\langle\Phi|H^+H^-\rangle|^2=0.58$ at $t=0$. As R decreases, the population of H^+H^- (or H^-H^+) becomes larger; however, the rate of ionization from a pure ionic state H^+H^- or H^-H^+ decreases owing to the greater attractive force of the distant nucleus exerted on the electron pair. At $R=1.6a_0$, $|\langle\Phi|H^+H^-\rangle|^2$ is large, but the electron cloud of Φ shrinks in comparison with H^+H^- or H^-H^+. We also note that the increase in $|\langle\Phi|H^+H^-\rangle|^2$ from $t=0$ to $t=3\pi/2\omega$ is only 0.16 for $R=1.6a_0$, while it is 0.35 for $R=4a_0$. This suggests that the unstable part of the existing H^-H^+ is smaller for $R=1.6a_0$ than for $R=4a_0$.

On the assumption that the ionization probability $P_I(t)$ is equal to $1-P_{init}(t)$ at $\varepsilon(t)=0$, we obtained $P_I(t=\pi/\omega)=0.000\,65$ and $P_I(t=2\pi/\omega)=0.072$. The value of $P_I(t=\pi/\omega)$ is regarded as an ionization probability for one half cycle at $f(t)=0.03E_H/ea_0$ ($I\approx 3\times10^{13}$ W/cm^2), which is the field amplitude averaged in the first half cycle. The ionization probability at $t=2\pi/\omega$ originates mainly from ionization in the second half cycle: $P_I(t=2\pi/\omega)$ is regarded as a half-cycle ionization probability at $f(t)=0.09E_H/ea_0$ ($I\approx 3\times10^{14}$ W/cm^2), which is the field amplitude averaged in the second half cycle. By fitting these half-cycle data to the form $P_I(t)=1-\exp(-\Gamma_I t)$, we can estimate the ionization rate Γ_I: $\Gamma_I\approx 0.000\,48$/fs at $f(t)=0.03E_H/ea_0$ and $\Gamma_I\approx 0.060$/fs at $f(t)=0.09E_H/ea_0$. We calculated ionization rates at various R and confirmed that the obtained ionization rate is smaller than the value for the corresponding static field of $\varepsilon(t)=f(t)=$const [53].

We next would like to extend the present half-cycle analysis to longer pulses that are more accessible to experimentalists. The wave function of the lowest vibrational $v=0$ state of H_2 has a peak around R_e. When the initial state is $v=0$, the ionization rate of real H_2 with moving nuclei will be

replaced with an ionization rate of H_2 at $R \approx R_e$. Here, we test the Γ_I obtained for $R=1.6a_0$ as the ionization rate of H_2 with moving nuclei. Using the Γ_I obtained, as an example, we estimated the ionization probability of H_2 interacting with a 25 fs *square* pulse ($\omega=0.06E_H/\hbar$). The estimated ionization probability $P_I(t=25$ fs) is only ~ 0.01 for $I \approx 3 \times 10^{13}$ W/cm^2 but increases to a value near unity (~ 0.78) for $I \approx 3 \times 10^{14}$ W/cm^2 (which is regarded as the saturation intensity). The great difference in the ionization probability between the two intensities is in accord with the experimental results [54] that for H_2 subject to 55 fs laser pulses of $\lambda = 750$ nm the appearance (threshold) intensity of the H_2^+ ion signal is $\sim 5 \times 10^{13}$ W/cm^2 and the saturation intensity $I_{\rm sat}$ is $\sim 2 \times 10^{14}$ W/cm^2.

At $I \approx 3 \times 10^{13}$ W/cm^2, the ionization rate Γ_I of H_2 at $R = 1.6a_0$ is larger than $\Gamma_{\rm H}$ by nearly one order of magnitude, where $\Gamma_{\rm H}$ is the ionization rate of H. Considering the fact that $I_p(H_2)=0.58E_H$ at $R=1.6a_0$ is even larger than $I_p({\rm H}) = 0.5E_H$, this implies that ionization in H_2 at $I \ll I_{\rm sat}$ is greatly enhanced by the electron-electron repulsion intensified in the localized ionic state.

3. $R=6a_0$ and $8a_0$

Snapshots of the reduced densities for $R=6a_0$ and $8a_0$ are shown in Figs. 3 and 4, respectively. The initial reduced densities for $R=6a_0$ and $8a_0$ shown in Figs. 3(a) and 4(a) indicate that the ground electronic state at large R is a state dominated by covalent character. For $R=6a_0$, $|\langle \Phi | {\rm H}^+{\rm H}^- \rangle|^2$ at $t=0$ is as small as 0.016; for $R=8a_0$, it further reduces to 6×10^{-4}. The reduced densities at $t=3\pi/2\omega=78.5\hbar/E_H$ for $R=6a_0$ and $8a_0$ are shown in Figs. 3(b) and 4(b), respectively.

The population of H^+H^- in an intense field becomes smaller as R increases. Around $t=3\pi/2\omega$, $|\langle \Phi | {\rm H}^+{\rm H}^- \rangle|^2$ is at most 0.06 for $R=6a_0$ and is very small, less than 0.004, for $R=8a_0$. The decrease in the H^+H^- population is unfavorable for tunnel ionization. In addition to the populations of H^+H^- and H^-H^+, there exists yet another factor that determines the ionization rate. The ratios of the relative ionization rate estimated at $t=2\pi/\omega$ to the maximum value of $|\langle \Phi | {\rm H}^+{\rm H}^- \rangle|^2$ around $t=3\pi/2\omega$ are 1.6, 50, 250, and 790 for $R=1.6a_0, 4a_0, 6a_0$ and $8a_0$, respectively; the ratio of the ionization rate to the population of H^+H^- (or H^-H^+) increases as R increases. One of the main reasons for this tendency is that the created H^+H^- becomes more unstable as R increases. The reduced density at $t=3.3\pi/2\omega=86.4\hbar/E_H$ for $R=6a_0$, which is just $8\hbar/E_H$ after the second peak of the field at $t=3\pi/2\omega$, is plotted in Fig. 3(c). The drastic change from Fig. 3(b) to 3(c) clearly shows the onset of rapid ionization from the created ionic state. A large part of the ionic component decays to Volkov states; that is, for $R \geq 6a_0$, the created H^+H^- ionizes completely within a half optical cycle (~ 1.27 fs). This is again consistent with Saenz's result [53] that the lifetime of pure H^+H^- in a static field with $\varepsilon = 0.06E_H/ea_0$ is shorter than 0.5 fs for $R \geq 6a_0$ (since the ionic and covalent states have no overlap at large R, each state can be assigned to an adiabatic state in a static field). For $R \geq 6a_0$, $|\langle \Phi | {\rm H}^+{\rm H}^- \rangle|^2$ reaches the maximum at about

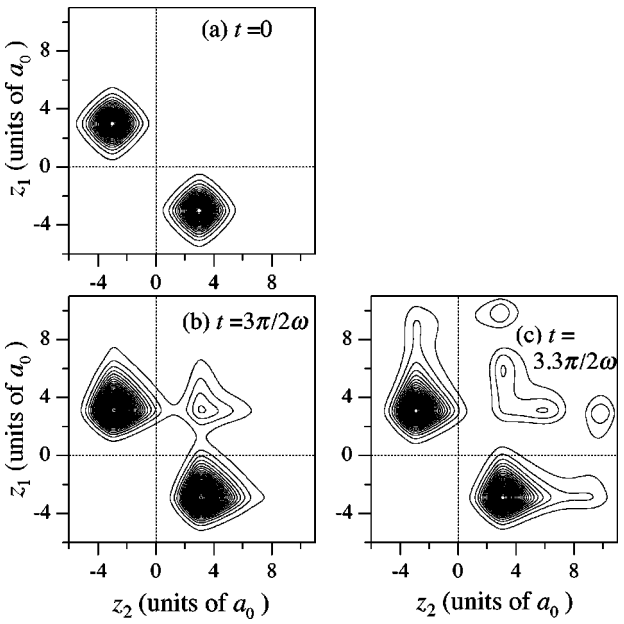

FIG. 3. Snapshots of the reduced density of H_2 at $R=6a_0$: (a) $t=0$, (b) $t=3\pi/2\omega$, (c) $t=3.3\pi/2\omega$. The change from (b) to (c) indicates rapid ionization from the created ionic state around $z_1=z_2=R/2$. The contour intervals in (b) and (c) are one-half of those in (a).

$20\hbar/E_H$ before the field reaches the local maximum at $t=3\pi/2\omega$, which reflects the rapid ionization of the created H^+H^- within a half optical cycle.

Another reason why the ratio of the ionization rate to the population $|\langle \Phi | {\rm H}^+{\rm H}^- \rangle|^2$ increases as R increases is the significant ionization from the covalent state at large R. Figure 3(b) and 3(c) shows that the ionizing currents from the ionic and covalent configurations for $R=6a_0$ are of the same order of magnitude. As mentioned previously, the ionization rate of a "pure" covalent state is small. For $R=6a_0$, the ionization rate of a covalent state in a static field with $\varepsilon = 0.06E_H/ea_0$ is about one-fourth as large as that of an ionic state (for $\varepsilon = 0.08E_H/ea_0$, one-tenth) [53]. On the other hand, as shown in Fig. 3, the remaining covalent component outmeasures the created ionic component $|\langle \Phi | {\rm H}^+{\rm H}^- \rangle|^2$, which is at most 0.06 around $t=3\pi/2\omega$. Therefore, for $R=6a_0$, as well as the ionization of the created localized ionic component, the direct ionization from the dominant covalent

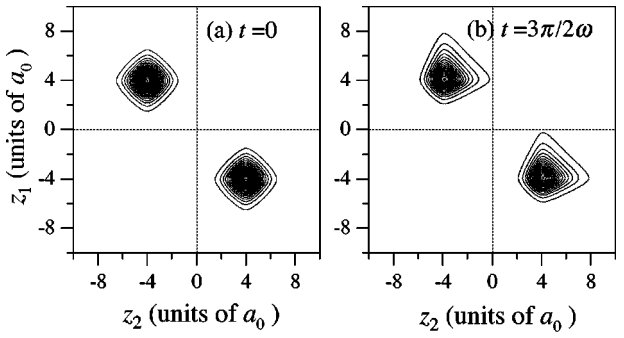

FIG. 4. Snapshots of the reduced density of H_2 at $R=8a_0$: (a) $t=0$, (b) $t=3\pi/2\omega$.

component significantly contributes to the total ionization probability.

For $R=8a_0$, as shown in Fig. 4(b), creation of an ionic state is greatly suppressed. As mentioned previously, $|\langle\Phi|H^+H^-\rangle|^2$ around $t=3\pi/2\omega$ is less than 0.004. Moreover, the ionization rate of an ionic state reaches a ceiling at large R ($\geqslant 6a_0$), where the attractive force exerted by the distant nuclei becomes negligible. The ionization rate from a covalent state is also almost independent of R if the field is strong enough to lower the ionization barrier of a H atom to the initial energy $-I_p(H)$. In this case, the ionization processes of two nearly isolated H atoms are triggered by one-electron motion and are independent of each other. The minimum field strength required for barrier suppression ionization of H is given by $I_P^2(H)/4 \approx 0.063 E_H/ea_0$. This is consistent with the result that the ionization rate of the covalent state is almost independent of R ($\geqslant 6a_0$) in a static field of $\varepsilon \geqslant 0.08 E_H/ea_0$ [53]. Hence, if the field strength is far beyond the barrier suppression strength of H, the ionization rate of the covalent state, as well as that of the ionic state, is almost independent of R: the main ionization route at large R ($>8a_0$) is a direct one from the dominant covalent component.

If the intensity is below a threshold value, for instance, if $\varepsilon(t)<0.04E_H/ea_0$ at $R=8a_0$, creation of an ionic state is inhibited, as will be discussed in Sec. III C: the dependence of the ionization rate on R is governed by the ionization rate of the covalent state. In a static field of $\varepsilon<0.04E_H/ea_0$, as R increases from $6a_0$, the ionization rate of the covalent state decreases up to $R\approx 10a_0$ [53]. This suggests that the polarization enhanced by two-electron correlation in the case of a weak field induces ionization from the covalent state. As R increases, this type of polarization diminishes; therefore, in the case of a weak field, the ionization rate of the covalent state decreases with increase in R up to a certain internuclear distance.

In conclusion, the main doorway state to ionization is the localized ionic state H^-H^+ or H^+H^-. As R increases, while the population of H^-H^+ decreases, a pure ionic state H^-H^+ becomes more unstable in a field because of the less attractive force of the distant nucleus. As a result, ionization is enhanced at the critical distance $R_c=(4-6)a_0$

B. Electrostatic consideration

In this subsection, the electronic dynamics of H_2 presented so far is discussed on the basis of an electrostatic model combined with a molecular orbital (MO) approximation. We consider the three representative electronic states: the zero-field ground state X and two ionic excited states $B\,^1\Sigma_u^+$ and EF [55]. The main electronic configurations involved in these states are three electronic configurations in the MO approximation, $(1s\sigma_g)^2$,$1s\sigma_g 2p\sigma_u$, and $(2p\sigma_u)^2$:

$$\phi_1=[a(1)a(2)+b(1)b(2)+a(1)b(2)+b(1)a(2)]/2, \tag{11a}$$

$$\phi_2=[a(1)a(2)-b(1)b(2)]/\sqrt{2}, \tag{11b}$$

$$\phi_3=[a(1)a(2)+b(1)b(2)-a(1)b(2)-b(1)a(2)]/2. \tag{11c}$$

Both ground and second excited configurations, ϕ_1 and ϕ_3, are linear combinations of ionic (aa,bb) and covalent ($ab+ba$) configurations, whereas ϕ_2 is purely ionic. The three configurations in Eqs. (11) are coupled by the large transition dipole moments $\langle\phi_1|(z_1+z_2)|\phi_2\rangle=\langle\phi_2|(z_1+z_2)|\phi_3\rangle=R/\sqrt{2}$. Under the condition in which the radiative interaction $R\varepsilon(t)/\sqrt{2}$ is much larger than the zero-field energy separations between electronic states, the diagonalization of the 3×3 instantaneous MO electronic Hamiltonian yields three field-following adiabatic states, i.e., the covalent state $(ab+ba)/\sqrt{2}$ and two localized ionic states (aa and bb) [43]. The lowering ionic state (aa or bb), where the two electrons are localized in the descending well, decreases in energy by the electrostatic energy shift $-|\varepsilon(t)|R$ of a charge displaced from nucleus to nucleus by the field, while the energy of the covalent state is relatively insensitive to the field strength. Therefore, when the energy shift $|\varepsilon(t)|R$ of $|H^+H^-\rangle$ (or $|H^+H^-\rangle$) is larger than the gap between the first excited ionic state and the ground state, the lowering ionic state and the covalent character-dominated initial state can cross each other in energy.

The initial ground state is adiabatically connected with the lowering ionic state after the crossing [43]. As the field strength increases, the lowest adiabatic state starting from the X state becomes more ionic. In the case of $R\leqslant 4a_0$, the energy gap at the avoided crossing between the lowest two adiabatic states is as large as that at zero field strengths because the transition dipole moment of the B-X transition, which enlarges the gap, increases as $\approx R/\sqrt{2}$ up to $R\approx 3a_0$. As a result, nonadiabatic transitions to upper adiabatic states hardly occur. Therefore, ionization occurs from the lowest adiabatic state directly to Volkov states.

In the case of relatively large R ($>R_e$), the field strength necessary for creating a localized ionic state, ε_t, can be estimated by adding the Coulomb attraction between H^+ and H^- in a localized ionic state. The energy of the initial covalent state is roughly given by $-2I_p(H)$. The energy of the localized ionic state in the descending well at the field $\varepsilon(t)$,$E(H^+H^-)$, is

$$E(H^+H^-)\approx -I_p(H)-I_p(H^-)-1/R-|\varepsilon(t)|R. \tag{12}$$

A necessary condition for the formation of a localized ionic state is then given by $E(H^+H^-)\leqslant -2I_p(H)$. We thus have the critical intensity ε_t as [43,56]

$$\varepsilon_t\approx[I_p(H)-I_p(H^-)-1/R]/R\approx[0.53-1/R]/R. \tag{13}$$

For $R=4a_0$, $\varepsilon_t=0.07E_H/ea_0$ is obtained. The dramatic increase in the population of H^+H^- shown in Fig. 1(d) can be explained by the fact that $|\varepsilon(t)|$ at $t=3\pi/2\omega, 0.09E_H/ea_0$, is greater than ε_t; on the other hand, for $|\varepsilon(t)|<\varepsilon_t$, the increase in the ionic character is small, as shown in Fig. 1(b).

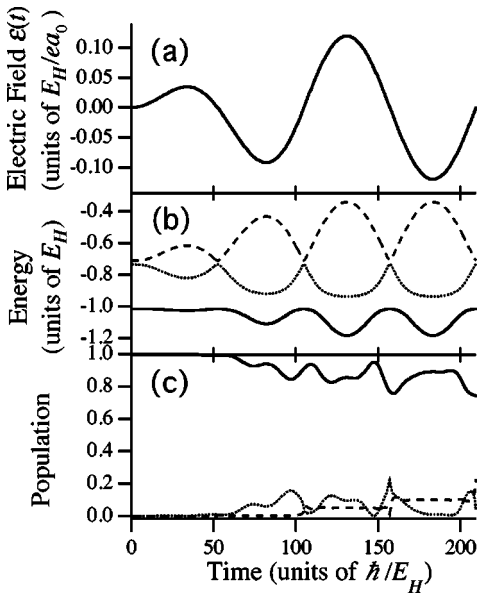

FIG. 5. Adiabatic state analysis of the electronic dynamics of H_2 at $R=4a_0$. The applied pulse used in Figs. 1–4 is plotted in (a). The effective instantaneous Hamiltonian is constructed from three main electronic states, *X*, *B*, and *EF*. The energies and populations of the three time-dependent adiabatic states $|1\rangle$, $|2\rangle$, and $|3\rangle$ of the 3×3 effective Hamiltonian are plotted in (b) and (c), respectively. In (b) and (c), the solid, dotted, and broken lines indicate the quantities for $|1\rangle$, $|2\rangle$, and $|3\rangle$, respectively. The gap at an avoided crossing is $0.17E_H$, which is almost as large as the zero-field gap ($\sim0.28E_H$). The probability of a nonadiabatic transition between the lowest two adiabatic states $|1\rangle$ and $|2\rangle$ is therefore small.

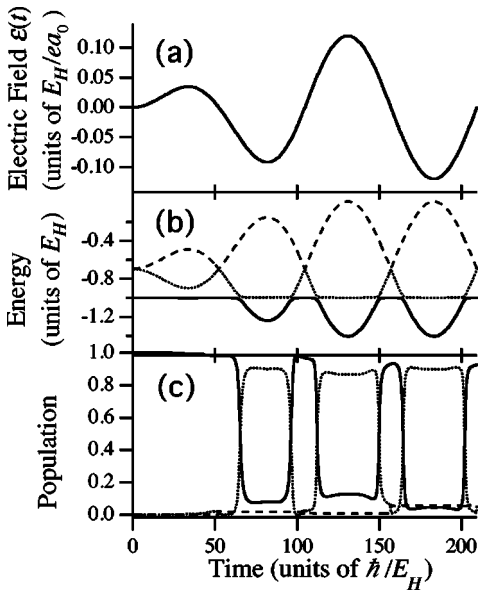

FIG. 6. Adiabatic state analysis of the electronic dynamics of H_2 at $R=6a_0$. The effective instantaneous Hamiltonian is constructed from the gerade and ungerade ionic states $|I_g\rangle$ and $|I_u\rangle$ in Eqs. (33) in addition to the ground electronic state *X*. The notations are the same as those in Fig. 5. As shown in (b), the energy difference between the lowest two adiabatic states $|1\rangle$ and $|2\rangle$ becomes smallest at $t_c=(65,97,112)\hbar/E_H$, etc. The gap between $|1\rangle$ and $|2\rangle$ at an avoided crossing, $0.037E_H$, is much smaller than that at $R=4a_0$: the probability of a nonadiabatic transition between $|1\rangle$ and $|2\rangle$ is large.

C. Adiabatic state analysis

Although Eq. (13) predicts the field strength necessary for crossing, to quantify the nonadiabatic crossing, we need to know the energy gaps at avoided crossings as well as the energy shifts of adiabatic states. In the following, we formulate the state dynamics of H_2 in terms of time-dependent adiabatic states. The formation of a localized ionic state can be quantified by using the eigenfunctions (adiabatic states) of an effective instantaneous Hamiltonian $H_{eff}(t)$ constructed from the representative three states *X*,*B*, and *EF*. We express the 3×3 effective Hamiltonian $H_{eff}(t)$ using the above three zero-field states as

$$H_{eff}(t)=\begin{pmatrix} E_X & -\mu_{X\text{-}B}\varepsilon(t) & 0 \\ -\mu_{X\text{-}B}\varepsilon(t) & E_B & -\mu_{B\text{-}EF}\varepsilon(t) \\ 0 & -\mu_{B\text{-}EF}\varepsilon(t) & E_{EF} \end{pmatrix}, \tag{14}$$

where E_X,E_B, and E_{EF} are the zero-field energies of the states *X*,*B*, and *EF*, respectively [55]. Here, $\mu_{X\text{-}B}$ is an effective transition moment between the states *X* and *B*, and $\mu_{B\text{-}EF}$ is an effective transition moment between *B* and *EF*.

Diagonalization of $H_{eff}(t)$ yields the time-dependent adiabatic states $\{|j\rangle\}$ and energies $\{E_j(t)\}$, where *j* runs from 1 to 3 in ascending order with respect to energy. The time-dependent Schrödinger equation for $H_{eff}(t)$,

$$i\partial|\Psi\rangle/\partial t=H_{eff}(t)|\Psi\rangle, \tag{15}$$

can be solved numerically. We then convert the state $|\Psi\rangle$ from the obtained zero-field basis expansion to an adiabatic state expansion as

$$|\Psi\rangle=\chi_1|1\rangle+\chi_2|2\rangle+\chi_3|3\rangle. \tag{16}$$

The populations of the adiabatic states, $\{|\chi_j|^2\}$, are obtained by projecting $|\Psi\rangle$ onto three states $|1\rangle$, $|2\rangle$, and $|3\rangle$ as $\chi_j=\langle j|\Psi\rangle$. The energies and populations of the three time-dependent adiabatic states for $R=4a_0$ and $6a_0$ are plotted in Figs. 5 and 6, respectively. The applied pulse is the same as that used in Figs. 1–4 and is plotted in Figs. 5(a) and 6(a).

1. $R=4a_0$

In the case of $R=4a_0$, the accurate theoretical values for the *X*-*B* and *B*-*EF* transition moments are used ($\mu_{X\text{-}B}=-1.433ea_0$ and $\mu_{B\text{-}EF}=-3.001ea_0$, respectively [55]). As shown in Fig. 5(b), the energy difference between the lowest two adiabatic states $|1\rangle$ and $|2\rangle$ becomes smallest at $t_c=(69,93,114)\hbar/E_H$, etc. The corresponding field strength is always $|\varepsilon(t_c)|=0.067E_H/ea_0$, which agrees fairly well with the value $\varepsilon_t=0.07E_H/ea_0$ obtained from Eq. (13). The gap at an avoided crossing is $0.17E_H$, which is on the order of the zero-field gap ($\sim0.28E_H$). The probability of a nonadiabatic transition between $|1\rangle$ and $|2\rangle$ is therefore small. As shown in Fig. 5(c), the nonadiabatic transition probability to

$|2\rangle$ for the avoided crossing at $t=69\hbar/E_H$ is only ~ 0.06. At small R ($\leqslant 4a_0$), the main pathway is certainly adiabatic: ionization proceeds through the lowest adiabatic state.

In Sec. III A, we have estimated the ionization probability from the quantity $1-P_{init}$, where P_{init} is the population of the initial state X at $\varepsilon(t)=0$. To be exact, however, this is only approximately valid. Besides $|1\rangle$, there exists a nonzero component of $|2\rangle$ at $\varepsilon(t_n=n\pi/\omega)=0$ (n being a positive integer). In the actual wave-packet simulation, the state $|2\rangle$ existing just after the preceding crossing at t_c is subjected to ionization (for instance, $t_{n=2}=105\hbar/E_H$ and $t_c=93\hbar/E_H$). At $\varepsilon(t)=0$, $|2\rangle$ is the state B. The ionization potential I_p of B is $0.19E_H$ at $R=4a_0$. The barrier suppression field strength $I_p^2/4$ for the corresponding one-electron atomic model is $0.009E_H/ea_0$. The field strength required for the crossing between $|1\rangle$ and $|2\rangle$ is $|\varepsilon(t_c)|=0.067E_H/ea_0$, which far exceeds the value of $I_p^2/4$. In a static field of $\varepsilon=0.06E_H/ea_0$, the ionization rate of $|2\rangle$ is as large as 2/fs [53]. These facts lead to an expectation that the state $|2\rangle$ is rapidly ionized. However, it takes only $12\hbar/E_H\approx 0.3$ fs ($=n\pi/\omega-t_c$) until the field returns to zero since the two states $|1\rangle$ and $|2\rangle$ cross each other at t_c. Thus, at least one-half of the $|2\rangle$ component existing at t_c remains when the field returns to zero (at $t_n=n\pi/\omega$). In the case of $R=4a_0$, therefore, the ionization probability deduced from $1-P_{init}$ is slightly overestimated.

The above three-state problem can be reduced to a two-state problem by prediagonalizing the 2×2 matrix consisting of the upper two states B and EF:

$$\begin{pmatrix} E_B & -\mu_{B\text{-}EF}\varepsilon(t) \\ -\mu_{B\text{-}EF}\varepsilon(t) & E_{EF} \end{pmatrix}. \tag{17}$$

Since $E_B\approx E_{EF}$, the eigenfunctions of the above matrix are nearly equal to the diabatic bases (containing localized ionic components)

$$(|B\rangle-|EF\rangle)/\sqrt{2}, \tag{18a}$$

$$(|B\rangle+|EF\rangle)/\sqrt{2}, \tag{18b}$$

and the eigenvalues are $E_B+\mu_{B\text{-}EF}\varepsilon(t)$ and $E_B-\mu_{B\text{-}EF}\varepsilon(t)$, respectively. Using the X state and the above two states represented by Eqs. (18), we can approximate $H_{eff}(t)$ as

$$H_{eff}(t)\approx \begin{pmatrix} E_X & \dfrac{-\mu_{X\text{-}B}\varepsilon(t)}{\sqrt{2}} & \dfrac{-\mu_{X\text{-}B}\varepsilon(t)}{\sqrt{2}} \\ \dfrac{-\mu_{X\text{-}B}\varepsilon(t)}{\sqrt{2}} & E_B+\mu_{B\text{-}EF}|\varepsilon(t)| & 0 \\ \dfrac{-\mu_{X\text{-}B}\varepsilon(t)}{\sqrt{2}} & 0 & E_B-\mu_{B\text{-}EF}|\varepsilon(t)| \end{pmatrix}. \tag{19}$$

The ratio of the coupling element $-\mu_{X\text{-}B}\varepsilon(t)/\sqrt{2}$ to the energy gap between the highest state and the ground state, $E_B-E_X-\mu_{B\text{-}EF}|\varepsilon(t)|$, is at most $\mu_{X\text{-}B}/\mu_{B\text{-}EF}$. This value is $\sim 1.4/3$ at $R=4a_0$ and becomes smaller as R increases. Thus, the effective Hamiltonian for the important nonadiabatic transition between the lowest two adiabatic states $|1\rangle$ and $|2\rangle$ can be given by

$$H'_{eff}(t)=\begin{pmatrix} E_X & -\mu_{X\text{-}B}\varepsilon(t)/\sqrt{2} \\ -\mu_{X\text{-}B}\varepsilon(t)/\sqrt{2} & E_B+\mu_{B\text{-}EF}|\varepsilon(t)| \end{pmatrix}. \tag{20}$$

The diabatic basis set used is $\{|X\rangle,(|B\rangle-|EF\rangle)/\sqrt{2}\}$ for $\varepsilon(t)>0$ and $\{|X\rangle,(|B\rangle+|EF\rangle)/\sqrt{2}\}$ for $\varepsilon(t)<0$.

The eigenfunctions $|1'\rangle$ and $|2'\rangle$ of $H'_{eff}(t)$ can be expressed in terms of

$$|a\rangle=[|X\rangle+(|B\rangle\pm|EF\rangle)/\sqrt{2}]/\sqrt{2}, \tag{21a}$$

$$|b\rangle=[|X\rangle-(|B\rangle\pm|EF\rangle)/\sqrt{2}]/\sqrt{2}, \tag{21b}$$

and

$$\theta=\arctan\left[\frac{E_X-E_B-\mu_{B\text{-}EF}|\varepsilon(t)|}{\pm\sqrt{2}\mu_{X\text{-}B}\varepsilon(t)}\right], \tag{22}$$

where the upper or lower sign should be taken according to whether $\varepsilon(t)$ is negative or positive. Using these expressions, we have, for $\varepsilon(t)<0$,

$$|1'\rangle=\cos\theta|a\rangle-\sin\theta|b\rangle, \tag{23a}$$

$$|2'\rangle=\cos\theta|b\rangle+\sin\theta|a\rangle, \tag{23b}$$

and, for $\varepsilon(t)<0$, $|1'\rangle$ and $|2'\rangle$ should be replaced with each other.

The eigenvalues of $H'_{eff}(t)$, E'_1 and E'_2, are given by

$$E'_{1,2}=\frac{1}{2}\{E_B+\mu_{B\text{-}EF}|\varepsilon(t)|+E_X \mp\sqrt{[E_B+\mu_{B\text{-}EF}|\varepsilon(t)|-E_X]^2+2|\mu_{X\text{-}B}\varepsilon(t)|^2}\}, \tag{24}$$

which fit well to the lowest two energies in Fig. 5(b). The gap

$$\Delta E'_{21}(t)=\sqrt{[E_B+\mu_{B\text{-}EF}|\varepsilon(t)|-E_X]^2+2|\mu_{X-B}\varepsilon(t)|^2} \tag{25}$$

reaches the minimum value of $0.16E_H/ea_0$ at $\varepsilon(t)=0.064E_H/ea_0$, which is nearly equal to the gaps at avoided crossings in Fig. 5(b). In the two-state model, the field strength required for the crossing, $\varepsilon(t'_c)$, is determined by the condition $d\Delta E'_{21}/d|\varepsilon(t)|=0$:

$$|\varepsilon(t'_c)|=-2\mu_{B\text{-}EF}(E_B-E_X)/2(\mu^2_{B\text{-}EF}+4\mu^2_{X\text{-}B}). \tag{26}$$

The agreement between $|\varepsilon(t_c)|=0.067E_H/ea_0$ and $|\varepsilon(t'_c)|=0.064E_H/ea_0$ is also good. The above expression provides a more accurate field strength required for the crossing than does ε_t.

The nonadiabatic transition between the lowest two adiabatic states $|1\rangle$ and $|2\rangle$ can be described well by the two-state model:

$$|\Psi\rangle\approx\chi'_1|1'\rangle+\chi'_2|2'\rangle. \tag{27}$$

Inserting the right-hand side of Eq. (27) into the time-dependent Schrödinger equation for $H'_{eff}(t)$, we obtain the coupled equations for the coefficients χ'_1 and χ'_2:

$$\frac{\partial}{\partial t}\chi'_1=-iE'_1(t)\chi'_1-\left(\frac{\partial\theta}{\partial t}\right)\chi'_2, \tag{28a}$$

$$\frac{\partial}{\partial t}\chi'_2=-iE'_2(t)\chi'_2-\left(\frac{\partial\theta}{\partial t}\right)\chi'_1, \tag{28b}$$

where the off-diagonal nonadiabatic coupling $\partial\theta/\partial t$ is given by

$$\frac{\partial\theta}{\partial t}=\frac{\mu_{X\text{-}B}(E_B-E_X)[d\varepsilon(t)/dt]}{\sqrt{2}[\Delta E'_{21}(t)]^2}, \tag{29}$$

which has a peak near each individual t_c.

In the adiabatic case where nonadiabatic transitions from $|1'\rangle$ hardly occur, the nonadiabatic coupling $\partial\theta/\partial t$ is always smaller than the gap $\Delta E'_{21}(t)$. This condition holds in the present case of $R=4a_0$; $\partial\theta/\partial t<0.07\hbar/E_H$ (for $f_0=0.12E_H/ea_0$) and $\Delta E'_{21}(t)>0.17E_H$. Then, the time duration τ_{tr} that the system exists in the transition region [57] is given by the temporal width of $\partial\theta/\partial t$ around t_c. The *full* width at half maximum of $\partial\theta/\partial t$, i.e., τ_{tr}, is less than the quarter cycle $\pi/2\omega$. The width decreases as the field envelope $f(t)$ or $|\mu_{B\text{-}EF}|$ increases. Since τ_{tr} for the crossing at $t_c=69\hbar/E_H$ is about $20\hbar/E_H$ ($\pi/2\omega=26\hbar/E_H$), the crossing is nearly isolated from the other ones, e.g., from that at $t_c=93\hbar/E_H$. For a short-time, isolated crossing, the diagonal energy gap in the 2×2 diabatic representation in Eq. (20), $\Delta E=E_B-E_X+\mu_{B\text{-}EF}|\varepsilon(t)|$, can be linearized with respect to time t; in addition, the off-diagonal matrix elements in Eq. (20) can be well approximated as constant elements evaluated at $t=t_c$. In this case, the nonadiabatic transition probability P'_{12} between $|1'\rangle$ and $|2'\rangle$ is given by the Landau-Zener formula [58]

$$P'_{12}=\exp[-2\pi v^2/|d\Delta E/dt|_{t=t_c}], \tag{30}$$

where the gradient $|d\Delta E/dt|$ and the constant off-diagonal element v at $t=t_c$ are given by

$$|d\Delta E/dt|_{t=t_c}=|\mu_{B\text{-}EF}d\varepsilon(t)/dt|_{t=t_c}, \tag{31}$$

$$v=-\mu_{X\text{-}B}\varepsilon(t_c)/\sqrt{2}. \tag{32}$$

The transition probability P'_{12} evaluated at $t_c=69\hbar/E_H$ is 0.064. This value is in good agreement with the population of $|2\rangle$ between $t_c=69\hbar/E_H$ and $93\hbar/E_H$ (~0.060), as shown in Fig. 5(c), which validates the present Landau-Zener formula, Eq. (30). As R decreases from $4a_0$, $v^2/|d\Delta E/dt|_{t=t_c}$ in Eq. (30) increases: the larger gap between the B and X states requires larger field strengths for crossing; in addition, the energy shift $[\propto R|\varepsilon(t)|]$ of the adiabatic states that have localized ionic components is small because of small R. Therefore, P'_{12} decreases with decrease in R. The two-state model shows that the main pathway is on the lowest adiabatic state in the region of small R ($\leqslant4a_0$). At small R ($\ll4a_0$), the ionization probability at $\varepsilon(t)=0$, P_I, is accurately estimated by $1-P_{init}$ because the bound component remaining at $\varepsilon(t)=0$ populates only the lowest adiabatic state, i.e., the initial state X.

To quantify the important ionic character, we define the gerade and ungerade mutually orthogonal ionic components as [43]

$$|I_g\rangle\equiv c_g(|\mathrm{H^+H^-}\rangle+|\mathrm{H^-H^+}\rangle), \tag{33a}$$

$$|I_u\rangle\equiv c_u(|\mathrm{H^+H^-}\rangle-|\mathrm{H^-H^+}\rangle), \tag{33b}$$

where c_g and c_u are the normalization constants ($c_g\approx0.675$ and $c_u\approx0.744$ at $R=4a_0$). In a range around $R=4a_0$, $|I_g\rangle$ is distributed between the X and EF states as ca. 0.34:0.66, while $|I_u\rangle$ is predominant in the B state ($|\langle B|I_u\rangle|^2\approx0.88$). Projecting the three states X, B, and EF onto Eqs. (33) for $|I_g\rangle$ and $|I_u\rangle$, we can estimate the localized ionic components in $|a\rangle$ and $|b\rangle$, i.e., in Eqs. (21). The localized ionic components in $|1'\rangle$ and $|2'\rangle$ are obtained by inserting $|a\rangle$ and $|b\rangle$ into Eqs. (23): at $t=3\pi/2\omega$, we have

$$|1'\rangle=0.99|a\rangle+0.12|b\rangle\propto0.85|\mathrm{H^+H^-}\rangle+0.24|\mathrm{H^-H^+}\rangle, \tag{34a}$$

$$|2'\rangle=0.99|a\rangle-0.12|b\rangle\propto-0.45|\mathrm{H^+H^-}\rangle+0.32|\mathrm{H^-H^+}\rangle. \tag{34b}$$

State $|1'\rangle$ represents the features of the wave packet in Fig. 1(d), i.e., that the localized ionic component $|\mathrm{H^+H^-}\rangle$ overwhelms the countercomponent $|\mathrm{H^-H^+}\rangle$ and is larger than the covalent components. This again confirms that ionization proceeds through a localized ionic component contained in the lowest adiabatic state in the case of small R ($\leqslant4a_0$). Considering the already ionized component at $t=3\pi/2\omega$, it

is reasonable that the localized ionic component involved in the wave packet, $|\langle\Phi(t=3\pi/2\omega)|H^+H^-\rangle|^2=0.54$, is smaller than $|\langle 1'|H^+H^-\rangle|^2=(0.85)^2=0.72$.

2. $R=6a_0$ and $8a_0$

As R increases from $4a_0$, Heitler-London-type H($n=1$)H($n=2$) atomic components such as $(1s)_r(2p_z)_l$ and $(1s)_r(2s)_l$ become predominant in the B state [55], where r and l designate the right and left protons, respectively. The component $(1s)_r(2p_z)_l$ is mainly responsible for the polarization (or field-induced deformation) of the covalent component. For example, as shown in Figs. 3(b) and 3(c), the covalent component takes an asymmetric shape with respect to the center $z_1=z_2=\pm R/2$ when $\varepsilon(t)\neq 0$. The three-state model using the X,B, and EF states can describe the polarization of the covalent components. On the other hand, these three states become less ionic as R increases from $4a_0$, although the ionic component predominates over a broad range up to $R=9a_0$ for the EF state [55]. It turns out that the three-state model is not appropriate for analyzing the dynamics concerning the ionic states at large R.

In order to pursue the dynamics of the ionic components at large R, we construct another type of effective Hamiltonian as follows. In an intermediate range around $R=4a_0$, the $|I_u\rangle$ component is mainly involved in the B state; as R increases, however, the overlap of the B state with $|I_u\rangle$ decreases. The point of constructing the effective Hamiltonian in the case of large R is to replace the B state in $H_{eff}(t)$ by $|I_u\rangle$. In short, the B state is formally forced to represent the role of the $|I_u\rangle$ component distributed among many excited states. The $|I_g\rangle$ component is distributed among X,EF, and other excited states. We treat the EF state as the representative state of the $|I_g\rangle$ component distributed among many excited states. Since the X state contains an $|I_g\rangle$ component, the present EF state is only allowed to have an ionic component as large as $\sqrt{1-|\langle X|I_g\rangle|^2}|I_g\rangle$.

On the basis of the above consideration, we propose replacing $\mu_{X\text{-}B}$ and $\mu_{B\text{-}EF}$ in Eq. (14) with the following effective transition moments:

$$\mu_{X\text{-}B}\Rightarrow -\langle I_u|(z_1+z_2)|X\rangle, \tag{35a}$$

$$\mu_{B\text{-}EF}\Rightarrow -\sqrt{1-|\langle X|I_g\rangle|^2}\langle I_g|(z_1+z_2)|I_u\rangle. \tag{35b}$$

No modifications to the energies E_X, E_B, and E_{EF} are made. The transition dipole moment between $|I_g\rangle$ and $|I_u\rangle$ is as large as $\langle I_g|(z_1+z_2)|I_u\rangle\approx R$.

We present an example of the state dynamics for the above-mentioned Hamiltonian. At $R=6a_0$, $\langle I_u|(z_1+z_2)|X\rangle=0.512a_0$ and $|\langle X|I_g\rangle|^2=0.0324$: as suggested in Eqs. (35), $\mu_{X\text{-}B}$ and $\mu_{B\text{-}EF}$ are replaced by the effective ones $-0.512ea_0$ and $-5.9ea_0$, respectively. Inserting the modified transition moments into the effective Hamiltonian Eq. (14), we solve the corresponding Schrödinger equation. The energies and populations of the obtained three adiabatic states for $R=6a_0$ are plotted in Fig. 6. As shown in Fig. 6(b), the energy difference between $|1\rangle$ and $|2\rangle$ becomes smallest at $t_c=(65,97,112)\hbar/E_H$, etc. The field strength at t_c is $|\varepsilon(t_c)|=0.051E_H/ea_0$. The value obtained from Eq. (13), $\varepsilon_t=0.06E_H/ea_0$, is roughly equal to $|\varepsilon(t_c)|$. The gap between $|1\rangle$ and $|2\rangle$ at an avoided crossing, $0.037E_H$, is much smaller than that at $R=4a_0$: the probability of a nonadiabatic transition between $|1\rangle$ and $|2\rangle$ is large. As shown in Fig. 6(c), the population of $|2\rangle$ created via the nonadiabatic transition through the avoided crossing at $t=65\hbar/E_H$ is as large as ~ 0.90.

It is shown in Fig. 6(c) that in addition to $|1\rangle$, there exists a nonzero component of $|2\rangle$ at $\varepsilon(t_n=n\pi/\omega)$. In the actual wave-packet simulation, which includes ionization, a large part of state $|2\rangle$ existing just after the previous crossing between $|1\rangle$ and $|2\rangle$ at t_c is ionized by the time at which the field $\varepsilon(t)=0$ returns to zero (for instance, $t_{n=2}=105\hbar/E_H$ and $t_c=97\hbar/E_H$). State $|2\rangle$, which is a localized ionic state just after the crossing, is ionized faster than in the case of $R=4a_0$ because the attractive force exerted by the distant nucleus is weaker at $R=6a_0$. Therefore, we can assume that the ionization probability P_I at $\varepsilon(t)=0$ is nearly equal to $1-P_{init}$ because then the population of any adiabatic state other than $|1\rangle$ is expected to be small. In small R ($<4a_0$) and large R ($>6a_0$) regions, P_I at $\varepsilon(t=n\pi/\omega)=0$ is expected to be equal to $1-P_{init}$. This is reinforced by the results for the 1D H_2 model showing that the agreement between P_I and $1-P_{init}$ at $\varepsilon(t=n\pi/\omega)=0$ is fairly good except in an intermediate region around $R=4a_0$.

The two-state model based on the formally same effective Hamiltonian as Eq. (20) can be used to described the nonadiabatic transition between $|1\rangle$ and $|2\rangle$. The basis functions are $\{|X\rangle,(|I_u\rangle-\sqrt{1-|\langle X|I_g\rangle|^2}|I_g\rangle)/\sqrt{2}\}$ for $\varepsilon(t)>0$ and $\{|X\rangle,(|I_u\rangle+\sqrt{1-|\langle X|I_g\rangle|^2}|I_g\rangle)/\sqrt{2}\}$ for $\varepsilon(t)<0$. The $|a\rangle$ and $|b\rangle$ in $|1'\rangle$ and $|2'\rangle$ are given by

$$|a\rangle=[|X\rangle+(|I_u\rangle\pm\sqrt{1-|\langle X|I_g\rangle|^2}|I_g\rangle)/\sqrt{2}]/\sqrt{2}, \tag{36a}$$

$$|b\rangle=[|X\rangle-(|I_u\rangle\pm\sqrt{1-|\langle X|I_g\rangle|^2}|I_g\rangle)/\sqrt{2}]/\sqrt{2}. \tag{36b}$$

The eigenfunctions $|1'\rangle$ and $|2'\rangle$ and eigenvalues E_1' and E_2' take the same forms as those of Eqs. (23) and (24), respectively. Using the two-state model formula Eq. (26), it is possible to calculate the field strength required for a level crossing as $|\varepsilon(t_c')|=0.051E_H/ea_0$, which is identical to $|\varepsilon(t_c)|$.

In the case of $R=6a_0$, there exists a period for which the nonadiabatic coupling $\partial\theta/\partial t$ is larger than the gap $\Delta E_{21}'(t)$. This is the case if the nonadiabatic transition between $|1'\rangle$ and $|2'\rangle$ is dominant (diabatic case). The transition time τ_{tr} is given by the period in which the inequality $(\partial\theta/\partial t)/\Delta E_{21}'(t)>1$ holds. The temporal width of $(\partial\theta/\partial t)/\Delta E_{21}'(t)$ around t_c is smaller than that of $\partial\theta/\partial t$. For the crossing around $t_c=65\hbar/E_H$, the range in which $(\partial\theta/\partial t)/\Delta E_{21}'(t)>1$ is satisfied is a time domain $t\approx(t_c\pm 3)\hbar/E_H$. Since the transition time $\tau_{tr}\approx 6\hbar/E_H$ is much shorter than the time differences between two consecutive crossings, the condition for an isolated transition holds. The short transition time is due to the large value ($\propto R$) of the effective transition moment Eq. (35b) replacing $|\mu_{B\text{-}EF}|$. For an isolated crossing, the nonadiabatic transition probability P_{12} is given by the Landau-Zener formula, Eq. (30), as be-

fore. In the case of $R=6a_0$, the transition probability P'_{12} evaluated at $t_c=65\hbar/E_H$ is 0.92. P'_{12} multiplied by the population of $|1\rangle$ (~ 0.98) just before the crossing at $t_c=65\hbar/E_H$ is equal to the population of $|2\rangle$ in the range between $t_c=65\hbar/E_H$ and $97\hbar/E_H$, which is ~ 0.90 as shown in Fig. 6(c).

We next show that around $t=3\pi/2\omega \approx 79\hbar/E_H$ the state $|1\rangle$ is a localized ionic state $|H^+H^-\rangle$, while $|2\rangle$ is covalent. As R increases, the two-state model becomes more accurate; the two states $|1'\rangle$ and $|2'\rangle$ become identical to $|1\rangle$ and $|2\rangle$, respectively. Using Eqs. (33) for $|I_g\rangle$ and $|I_u\rangle$, we can estimate the localized ionic components of $|a\rangle$ and $|b\rangle$ in Eqs. (36) ($c_g \approx 0.7044$ and $c_u \approx 0.7098$ at $R=6a_0$). Inserting $|a\rangle$ and $|b\rangle$ into Eqs. (23), we obtain $|1'\rangle$ and $|2'\rangle$ at $t=3\pi/2\omega$ as

$$|1'\rangle \propto |H^+H^-\rangle, \tag{37a}$$

$$|2'\rangle \propto -0.042|H^+H^-\rangle + 0.13|H^-H^+\rangle, \tag{37b}$$

which means that $|1\rangle$ is $|H^+H^-\rangle$ and $|2\rangle$ is covalent. Since the population of $|2\rangle$, P_2, is ~ 0.90 at $t \approx 3\pi/2\omega$, the covalent component outmeasures the ionic component. This is consistent with the wave-packet dynamics shown in Fig. 3. Since $P_1(t=3\pi/2\omega) \approx 0.08$, the population of $|H^+H^-\rangle$ in the dynamics based on the two- or three-state model is also ~ 0.08. Considering the prompt ionization of H^+H^- formed around $t=3\pi/2\omega$, it is reasonable that the localized ionic component involved in the wave packet, $|\langle \Phi(t=3\pi/2\omega)|H^+H^-\rangle|^2 \approx 0.04$, is smaller than the value ~ 0.08.

At $R=8a_0$, $\langle I_u|(z_1+z_2)|X\rangle = 0.15a_0$ and $|\langle X|I_g\rangle|^2 = 0.001\,15$; $\mu_{X\text{-}B}$ and $\mu_{B\text{-}EF}$ are replaced with the effective values $-0.15ea_0$ and $-8.00ea_0$, respectively. The energy difference between the lowest two adiabatic states $|1\rangle$ and $|2\rangle$ becomes smallest at $t_c=(63,99,111)\hbar/E_H$, etc. The corresponding field strength is $|\varepsilon(t_c)|=0.043E_H/ea_0$ $[=|\varepsilon(t'_c)|]$. The gap between $|1\rangle$ and $|2\rangle$ at an avoided crossing is as small as $0.01E_H$: the probability of a nonadiabatic transition between $|1\rangle$ and $|2\rangle$ is very large. The Landau-Zener value P'_{12} (~ 0.996) multiplied by the population of $|1\rangle$ ($P_1 \approx 0.996$) just before the crossing at $t_c=63\hbar/E_H$ is equal to $P_2 \approx 0.993$ in the range between $t_c=63\hbar/E_h$ and $99\hbar/E_H$. Since the lowest adiabatic state $|1\rangle \approx |1'\rangle$ is $|H^+H^-\rangle$, the population of $|H^+H^-\rangle$ in the dynamics based on the two- or three-state model is very small as $P_1(t=3\pi/2\omega) \approx 0.004$ (in the wave-packet dynamics, $|\langle \Phi|H^+H^-\rangle|^2 \approx 0.001$ at $t=3\pi/2\omega$). This means that ionic components are scarcely involved, i.e., the main pathway is the diabatic one tracing the covalent character-dominated state, which is consistent with the wave-packet dynamics shown in Fig. 4.

IV. SUMMARY AND CONCLUDING REMARKS

The tunnel ionization of H_2 in an intense laser field ($I \approx 10^{14}$ W cm^{-2} and $\lambda = 760$ nm) has been examined with accurate evaluation of two-electron dynamics by the dual transformation method. The molecular axis is assumed to be parallel to the polarization direction of the applied laser field. We have estimated the ionization probabilities at different values of R to reveal the mechanism of enhanced ionization in a two-electron molecular system. An ionic component characterized by the electronic structure H^+H^- or H^-H^+ is created near the descending well owing to laser-induced electron transfer from the ascending well. Ionization proceeds via the formation of a localized ionic component in the *descending* well, in contrast to the H_2^+ case, where the electron is ejected most easily from the *ascending* well. As R increases, while the population of H^-H^+ decreases, a pure ionic state H^-H^+ becomes more unstable in an intense field because of the less attractive force of the distant nucleus. As a result, ionization is enhanced at the critical distance $R_c=(4\text{–}6)a_0$. Although H_2 in the ground vibrational state does not expand to R_c [45], the peak of the ionization probability around R_c indicates that ionization will be strongly enhanced when H_2 is vibrationally excited.

We have estimated that the change in R from $1.6a_0$ to $4a_0$ would enhance the ionization rate by a factor of 10–20. In the small R ($\leqslant 4a_0$) region, the main doorway state to ionization is identical to the localized ionic state H^-H^+ or H^+H^-. Around $R=6a_0$, the ionization from the covalent state competes with that from the created localized ionic state. As R increases further, the electron density transferred between the nuclei is suppressed: the main character becomes covalent. Although the rate of direct ionization from a covalent state is much smaller than that from an ionic state, the ionization at large R ($\geqslant 8a_0$) mainly proceeds from the remaining covalent component.

Recently, Nibarger *et al.* suggested that the ionization rate of a charge-asymmetric pathway of N_2 can greatly exceed that of a charge-symmetric pathway [18]. For example, an asymmetric pathway is the ionization from (1, 2) to (1, 3) and a symmetric pathway is the ionization from (1, 2) to (2, 2), where (n,m) stands for an $n+m$ charged state leading to the dissociation channel $N_2^{(n+m)+} \rightarrow N^{n+} + N^{m+}$. Their experimental results indicate that at small internuclear distances ($R \sim 4a_0$) the rate of the ionization from (1, 2) to (1, 3) is larger than that to (2, 2). This is explained well by the mechanism proposed in this paper that ionization is enhanced by field-induced intramolecular electron transfer; that is, the first step is the adiabatic intramolecular electron transfer from (1, 2) to (0, 3) and ionization then proceeds from the created neutral site to (1, 3). In intense fields, the higher (0, 3) channel is expected to cross the (1, 2) channel. According to the electrostatic consideration in Sec. III B, the energy difference between the (0, 3) and (1, 2) channels is estimated as $-R\varepsilon(t)-2/R+I_p(N^{2+})-I_p(N)$, which can be negative in high-intensity fields ($I > 10^{15}$ W cm^{-2}). Their report that the asymmetric channel is created at a smaller internuclear distance is consistent with our findings that adiabatic intramolecular electron transfer occurs preferentially at smaller internuclear distances (if the relevant two states can cross each other). As R increases, the (2, 2) channel becomes open. To explain this observation, we propose a mechanism due to electron localization (nonadiabatic transfer). The N^{1+} site of the (1, 2) channel is located at the descending well (lower-

energy side) at small R, but the N^{1+} site switches over to the ascending well at large R: as R increases, electron transfer becomes suppressed. As in the H_2^+ case, one of the electrons trapped in the unstable ascending well can be easily ejected over the inner and outer barriers: the N^{1+} site turns a N^{2+} site of the (2, 2) channel.

We have also investigated the intramolecular electronic dynamics that governs the ionization process by analyzing the populations of field-following adiabatic states defined as eigenfunctions of the instantaneous electronic Hamiltonian. In a high-intensity and low-frequency regime, only a limited number of adiabatic states participate in the intramolecular electronic dynamics, i.e., dynamics of bound electrons. The effective instantaneous Hamiltonian for H_2 is constructed from three main electronic states, X, B, and EF (at large R, the last two electronic states are replaced with the ungerade and gerade ionic states). By solving the time-dependent Schrödinger equation for the 3×3 effective Hamiltonian, we have found that the difference in electronic and ionization dynamics between the small R case and the large R case originates in the character of the level crossing of the lowest two adiabatic states.

As the field strength increases, the lowering second lowest adiabatic state $|2\rangle$ comes closer to the lowest adiabatic state $|1\rangle$ starting from the X state. The transition period in which a nonadiabatic transition between $|1\rangle$ and $|2\rangle$ is completed is much smaller than the quarter optical cycle $\pi/2\omega$. Thus, a nonadiabatic transition is localized around the time t_c when the field strength $\varepsilon(t)$ reaches the value required for a crossing, $\varepsilon(t_c)$. In the case of $R\leqslant4a_0$, the energy gap at the avoided crossing between $|1\rangle$ and $|2\rangle$ is as large as that at zero field strengths. As a result, nonadaiabtic transitions to upper adiabatic states hardly occur. When $|\varepsilon(t)|$ is larger than $|\varepsilon(t_c)|$, $|1\rangle$ is ionic, while $|2\rangle$ is covalent. Therefore, ionization occurs from state $|1\rangle$ characterized by a localized ionic state H^+H^- or H^-H^+ directly to Volkov states. In the case of large R ($>4a_0$), nonadiabatic transitions occur from $|1\rangle$ to $|2\rangle$ when these two states cross each other. For $R>6a_0$, ionization proceeds mainly through state $|2\rangle$, which is a covalent character-dominated state when $|\varepsilon(t)|>|\varepsilon(t_c)|$.

The three-state problem can be reduced to a two-state problem by prediagonalizing the 2×2 matrix constructed in terms of the upper two states B and EF. On the basis of the two-state model, an analytical expression of the field strength required for the crossing of $|1\rangle$ and $|2\rangle$ is derived; moreover, the probability of a nonadiabatic transition between $|1\rangle$ and $|2\rangle$ is expressed by the Landau-Zener formula. The results based on these simple formulas agree with those in the three-state treatment.

The characteristic features of electronic dynamics of H_2 in an intense laser field lead to a simple electrostatic view that each atom in a molecule is charged by field-induced electron transfer and ionization proceeds via the most unstable (most negatively charged) atomic site. The success of the adiabatic state analysis for H_2 originates from the fact that the dynamics of bound electrons and the subsequent ionization process can be clarified in terms of a small number of ''field-following'' adiabatic states. The properties of adiabatic states of multielectron molecules can be calculated by *ab initio* MO methods. While the time-dependent adiabatic potentials calculated by the MO method are used to evaluate the nuclear dynamics (such as bond stretching) until the next ionization process, the charge distributions on individual atomic sites are used to estimate the ionization probability. We have already applied this approach to a multielectron polyatomic molecule, CO_2, in an intense field [31,32] and revealed that in the CO_2^{2+} stage the two C—O bonds can be symmetrically (concertedly) stretched while accompanied by a large-amplitude bending motion. This approach is simple but it has wide applicability in predicting the *electronic* and *nuclear* dynamics of polyatomic molecules in intense laser fields.

ACKNOWLEDGMENTS

This work was supported in part by the Development of High-Density Optical Pulse Generation and Advanced Material Control Techniques and by grants-in-aid for scientific research from the Ministry of Education, Culture, Sports, Science and Technology, Japan (Grants No. 12640484 and No. 14540463).

[1] J.H. Eberly, J. Javanainen, and K. Rzążewski, Phys. Rev. A **51**, 1495 (1991).
[2] *Atoms in Intense Laser Fields*, edited by M. Gavrila (Academic Press, New York, 1992).
[3] V.P. Krainov, H.R. Reiss, and B.M. Smirnov, *Radiative Processes in Atomic Physics* (Wiley, New York, 1997).
[4] K. Burnett, V.C. Reed, J. Cooper, and P.L. Knight, Phys. Rev. A **45**, 3347 (1992); J.L. Krause, K.J. Schafer, and K.C. Kulander, *ibid.* **45**, 4998 (1992); T. Zuo, A.D. Bandrauk, M. Ivanov, and P.B. Corkum, *ibid.* **51**, 3991 (1995).
[5] A. Rundquist, G. Durfee III, Z. Chang, C. Herne, S. Backus, M.M. Murnane, and H.C. Kapteyn, Science **280**, 1412 (1998); T. Brabec and F. Krausz, Rev. Mod. Phys. **72**, 545 (2000).
[6] L.V. Keldysh, Sov. Phys. JETP **20**, 1307 (1965).
[7] M.J. Dewitt, and R.J. Levis, Phys. Rev. Lett. **81**, 5101 (1998); J. Chem. Phys. **108**, 7739 (1998).
[8] P.B. Corkum, Phys. Rev. Lett. **71**, 1994 (1993).
[9] M.V. Ammosov, N.B. Delon, and V.P. Krainov, Sov. Phys. JETP **64**, 1191 (1986).
[10] T.D.G. Walsh, F.A. Ilkov, and S.L. Chin, J. Phys. B **30**, 1191 (1997).
[11] Th. Weber, H. Giessen, M. Weckenbrock, G. Urbasch, A. Staudte, L. Spielberger, O. Jagutzki, V. Mergel, M. Vollmer, and R. Dörner, Science **405**, 658 (2000); R. Dörner, V. Mergel, O. Jagutzki, L. Spielberger, J. Ullrich, R. Moshammer, and H. Schmidt-Böcking, Phys. Rep. **330**, 95 (2000).
[12] R. Moshammer *et al.*, Phys. Rev. A **65**, 035401 (2002).
[13] M.Y. Kuchiev, J. Phys. B **28**, 5093 (1995).

[14] A. Becker and F.H.M. Faisal, Phys. Rev. Lett. **84**, 3546 (2000).
[15] K.T. Taylor, J. Parker, D. Dundas, E. Smyth, and S. Vitirito, Laser Phys. **9**, 98 (1999).
[16] C. Cornaggia, J. Lavancier, D. Normand, J. Morellec, P. Agostini, J.P. Chambaret, and A. Antonetti, Phys. Rev. A **44**, 4499 (1991); J.H. Posthumus, K. Codling, L.J. Frasinski, and M.R. Thompson, Laser Phys. **7**, 813 (1997).
[17] G.N. Gibson, M. Li, C. Guo, and J.P. Nibarger, Phys. Rev. A **58**, 4723 (1998).
[18] J.P. Nibarger, S.V. Menon, and G.N. Gibson, Phys. Rev. A **63**, 053406 (2001).
[19] B. Friedrich and D. Herschbach, Phys. Rev. Lett. **74**, 4623 (1995); H. Sakai, C.P. Safvan, J.J. Larsen, K.M. Hillgs, K. Hald, and H. Stapelfeldt, J. Chem. Phys. **110**, 10 235 (1999); J.J. Larsen, H. Sakai, C.P. Safvan, Ida Wendt-Larsen, and H. Stapelfeldt, *ibid.* **111**, 7774 (1999).
[20] J.P. Nibarger, M. Li, S.V. Menon, and G.N. Gibson, Phys. Rev. Lett. **83**, 4975 (1999).
[21] L. Quaglia and C. Cornaggia, Phys. Rev. Lett. **84**, 4565 (2000).
[22] J.H. Posthumus, A.J. Giles, M.R. Thompson, and K. Codling, J. Phys. B **29**, 5811 (1996); L.J. Frasinski, K. Codling, and P. Hatherly, Phys. Rev. Lett. **58**, 2424 (1989); K. Codling and L.J. Frasinski, J. Phys. B **26**, 783 (1993).
[23] E. Constant, H. Stapelfelt, and P.B. Corkum, Phys. Rev. Lett. **76**, 4140 (1996).
[24] C. Cornaggia, J. Lavancier, D. Normand, J. Morellec, and H.X. Liu, Phys. Rev. A **42**, 5464 (1990); M. Schmidt, D. Normand, and C. Cornaggia, *ibid.* **50**, 5037 (1994).
[25] Ph. Hering and C. Cornaggia, Phys. Rev. A **57**, 4572 (1998).
[26] I. Kawata, H. Kono, and A.D. Bandrauk, Phys. Rev. A **64**, 043411 (2001).
[27] K. Harumiya, I. Kawata, H. Kono, and Y. Fujimura, J. Chem. Phys. **113**, 8953 (2000).
[28] I. Kawata, H. Kono, and Y. Fujimura, J. Chem. Phys. **110**, 11152 (1999); Chem. Phys. Lett. **289**, 546 (1998).
[29] H. Kono and H. Kawata, in *Advances in Multi-Photon Processes and Spectroscopy*, edited by R. J. Gordon and Y. Fujimura (World Scientific, Singapore, 2001), Vol. 14, p. 165.
[30] H. Kono, K. Harumiya, Y. Fujimura, and I. Kawata, in *Photonic, Electronic and Atomic Collisions (XXII ICPEAC)*, edited by C.R. Vane (Rinton, Princeton, 2001).
[31] H. Kono and S. Koseki, in *Laser Control and Manipulation of Molecules*, ACS Symposium Series, edited by A. D. Bandrauk, R. J. Gordon, and Y. Fujimura (ACS, Oxford, 2002), Vol. 821 p. 267.
[32] H. Kono, S. Koseki, M. Shiota, and Y. Fujimura, J. Phys. Chem. A **105**, 5627 (2001).
[33] A. Hishikawa, A. Iwamae, and K. Yamanouchi, Phys. Rev. Lett. **83**, 1127 (1999); A. Iwamae, A. Hishikawa, and K. Yamanouchi, J. Phys. B **33**, 223 (2000).
[34] S. Shimizu, J. Kou, S. Kawato, K. Shimizu, S. Sakabe, and N. Nakashima, Chem. Phys. Lett. **317**, 609 (2000).
[35] A different analysis of the measured kinetic energies of fragment ions was proposed in Ref. [18]. The internuclear distance at the moment of ionization deduced from the analysis of N_2 can be smaller than R_c but is much larger than R_e for high-charge states.
[36] T. Zuo and A.D. Bandrauk, Phys. Rev. A **48**, 3837 (1993); S. Chelkowski and A.D. Bandrauk, J. Phys. B **28**, L273 (1999).
[37] T. Seidemann, M.Y. Ivacov, and P.B. Corkum, Phys. Rev. Lett. **75**, 2819 (1995).
[38] A.D. Bandrauk, Comments At. Mol. Phys. D **1**, 97 (1999); A.D. Bandrauk and J. Ruel, Phys. Rev. A **59**, 2153 (1999).
[39] Ionization rates of H_2^+ in static fields, as well as adiabatic energies, have also been calculated by complex scaling methods. See, e.g., Z. Mulyukov, M. Pont, and R. Shakeshaft, Phys. Rev. A **54**, 4299 (1996); M. Plummer and J.F. McCann, J. Phys. B **29**, 4625 (1996).
[40] A. Zavriyev, P.H. Bucksbaum, J. Squier, and F. Saline, Phys. Rev. Lett. **70**, 1077 (1993); B. Sheehy and L.F. DiMauro, Annu. Rev. Phys. Chem. **47**, 463 (1996).
[41] T.D.G. Walsh, F.A. Ilkov, S.L. Chin, F. Châteauneuf, T.-T. Nguyen-Daug, S. Chelkowski, A.D. Bandrauk, and O. Atabek, Phys. Rev. A **58**, 3922 (1998); T.-T. Nguyen-Daug, F. Châteauneuf, S. Manoli, O. Atabek, and A. Keller, *ibid.* **56**, 2142 (1997).
[42] H. Yu, T. Zuo, and A.D. Bandrauk, Phys. Rev. A **54**, 3290 (1996).
[43] I. Kawata, H. Kono, Y. Fujimura, and A.D. Bandrauk, Phys. Rev. A **62**, 031401(R) (2000); I. Kawata, A.D. Bandrauk, H. Kono, and Y. Fujimura, Laser Phys. **11**, 181 (2001).
[44] C. Guo, M. Li, J.P. Nibarger, and G.N. Gibson, Phys. Rev. A **61**, 033413 (2000).
[45] M. Lein, T. Kreibich, and V. Engel, Phys. Rev. A **65**, 033403 (2002).
[46] C. Cornaggia and Ph. Hering, Phys. Rev. A **62**, 023403 (2000).
[47] Other approaches commonly used are classical mechanical approaches and time-dependent Thomas-Fermi models. See, for example, K. Ishikawa and T. Blemski, Phys. Rev. A **61**, 063408 (2000); M. Brewczyk and K. Rzążewski, *ibid.* **61**, 023412 (2000).
[48] I. Kawata and H. Kono, J. Chem. Phys. **111**, 9498 (1999); H. Kono, A. Kita, Y. Ohtsuki, and Y. Fujimura, J. Comput. Phys. **130**, 148 (1997).
[49] K.C. Kulander, K.J. Schafer, and J.L. Krause, [2], p. 247; K.J. Schafer, and K.C. Kulander, Phys. Rev. Lett. **78**, 638 (1997).
[50] X. Chu and S.I. Chu, Phys. Rev. A **63**, 023411 (2001).
[51] *Computational Methods in Partial Differential Equations*, edited by A.R. Mitchell (Wiley, New York, 1969).
[52] M.D. Feit, J.A. Fleck, Jr., and A. Steiger, J. Comput. Phys. **47**, 412 (1982); M.D. Feit, and J.A. Fleck, Jr., J. Chem. Phys. **78**, 301 (1983).
[53] A. Saenz, Phys. Rev. A **61**, 051402 (2000).
[54] M.R. Thompson, M.K. Thomas, P.F. Taday, J.H. Posthumus, A.J. Langley, L.J. Frasinski, and K. Codling, J. Phys. B **30**, 5575 (1996).
[55] W. Kołos and L. Wolniewicz, J. Chem. Phys. **43**, 2429 (1965); **45**, 509 (1966); L. Wolniewicz, *ibid.*, **51**, 5002 (1969); L. Wolniewicz and K. Dressler, *ibid.*, **82**, 3292 (1985).
[56] A.D. Bandrauk, in *The Physics of Electronic and Atomic Collisions*, edited by Y. Itikawa, K. Okuno, H. Tanaka, A. Yagishita, and M. Matsuzawa, AIP Conf. Proc. No. 500 (AIP, Melville, NY, 1999), p. 102.
[57] Y. Kayanuma, J. Phys. Soc. Jpn. **53**, 108 (1984); K. Mullen, E. Ben-Jacob, Y. Gefen, and Z. Schuss, Phys. Rev. Lett. **62**, 2543 (1989).
[58] C. Zener, Proc. R. Soc. London, Ser. A **137**, 127 (1932); C. Zhu, Y. Teranishi, and H. Nakamura, Adv. Chem. Phys. **117**, 127 (2001).